Article

pubs.acs.org/Biomac

Imparting Superhydrophobicity to Biodegradable Poly(lactide-*co*-glycolide) Electrospun Meshes

Jonah A. Kaplan,[†] Hongyi Lei,[‡] Rong Liu,[‡] Robert Padera,[§] Yolonda L. Colson,[‡] and Mark W. Grinstaff*[,†]

[†]Departments of Biomedical Engineering and Chemistry, Boston University, Boston, Massachusetts 02215, United States

[‡]Department of Surgery and [§]Department of Pathology, Brigham and Women's Hospital, 75 Francis Street, Boston, Massachusetts 02115, United States

Supporting Information

ABSTRACT: The synthesis of a family of new poly(lactic acid-*co*-glycerol monostearate) (PLA–PGC_{18}) copolymers and their use as biodegradable polymer dopants is reported to enhance the hydrophobicity of poly(lactic acid-*co*-glycolic acid) (PLGA) nonwoven meshes. Solutions of PLGA are doped with PLA–PGC_{18} and electrospun to form meshes with micrometer-sized fibers. Fiber diameter, percent doping, and copolymer composition influence the nonwetting nature of the meshes and alter their mechanical (tensile) properties. Contact angles as high as 160° are obtained with 30% polymer dopant. Lastly, these meshes are nontoxic, as determined by an NIH/3T3 cell biocompatibility assay, and displayed a minimal foreign body response when implanted in mice. In summary, a general method for constructing biodegradable fibrous meshes with tunable hydrophobicity is described for use in tissue engineering and drug delivery applications.

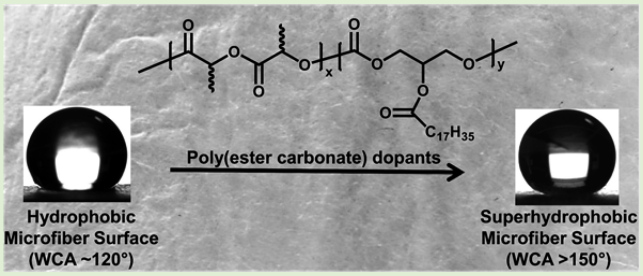

INTRODUCTION

Aliphatic biodegradable polyesters, such as poly(lactic acid) (PLA), poly(glycolic acid) (PGA), and poly(lactic acid-*co*-glycolic acid) (PLGA), are widely used polymers in the clinic and biomedical research because they are nontoxic, biodegradable, and readily synthesized.[1] Since the introduction of PGA and PLGA sutures in the 1960s and early 1970s, respectively,[2−5] these poly(hydroxy acids) are easily processed into a variety of additional application-specific form factors such as micro-[6,7] and nanoparticles,[8,9] wafers/discs,[10] meshes,[11] foams,[12] and films.[13] Copolymers consisting of lactic acid and glycolic acid are of particular interest because varying the monomer composition allows for control of the crystallinity, mechanical strength, and degradation rate.[14,15] Other approaches to alter these material properties, to facilitate cell adhesion, or to improve drug diffusion kinetics include synthesizing copolymers using functionalizable[16−18] or bioactive[19] comonomers and modifying the hydrophobicity/hydrophilicity via changes in surface texture, morphology, and form factor (fibers vs cast films) of the resulting material.

Material surfaces that exhibit extreme hydrophobicity or superhydrophobicity possess an apparent contact angle of >150°. These surfaces are fabricated by introducing high surface roughness to a low-surface-energy material in order to maintain a stable air−liquid−solid interface that resists wetting.[20] Superhydrophobic materials are commonly observed in nature, and synthetic analogues have been developed that possess water-repellant, self-cleaning, and drag-resistant surface properties.[21] From a biomaterials perspective, these materials are being explored for minimizing biofouling (e.g., reducing protein adsorption, cell adhesion, and cell proliferation)[22−25] and for drug delivery applications,[26−29] including those that are triggered by ultrasound.[30] Synthetic superhydrophobic materials are fabricated using various top-down and bottom-up approaches, such as micropatterning/microtexturing,[31] electrospraying,[32,33] solvent-induced polymer crystallization,[34] and electrospinning.[21,35,36] In electrospinning, a continuous fiber jet is ejected from the needle tip of a syringe containing a polymer solution, which is driven by the balancing of surface tension and electrostatic (repulsive) forces under an applied high voltage. The electrospinning approach to constructing superhydrophobic materials is particularly attractive because it results in nano- or microfiber meshes with high surface areas, porosity, and surface roughness while also providing mechanical integrity and three-dimensionality.

For controlled drug delivery applications, the entrapped air in superhydrophobic three-dimensional materials acts as a metastable barrier to water infiltration and controls drug release.[27−29] Thus, the development of these materials for this application requires not only tuning the rate of drug delivery via the metastable state but also controlling their chemical, physical, and mechanical properties. Previous work on superhydrophobic drug eluting electrospun meshes used poly(ε-caprolactone) (PCL) as the major polymer constitutent. PCL is a hydrophobic polyester that degrades slowly in the human body (~2 to 3 years) compared to that of other

Received: March 17, 2014
Revised: May 28, 2014
Published: June 5, 2014

Scheme 1. Synthesis of Poly(ester carbonate) Copolymers

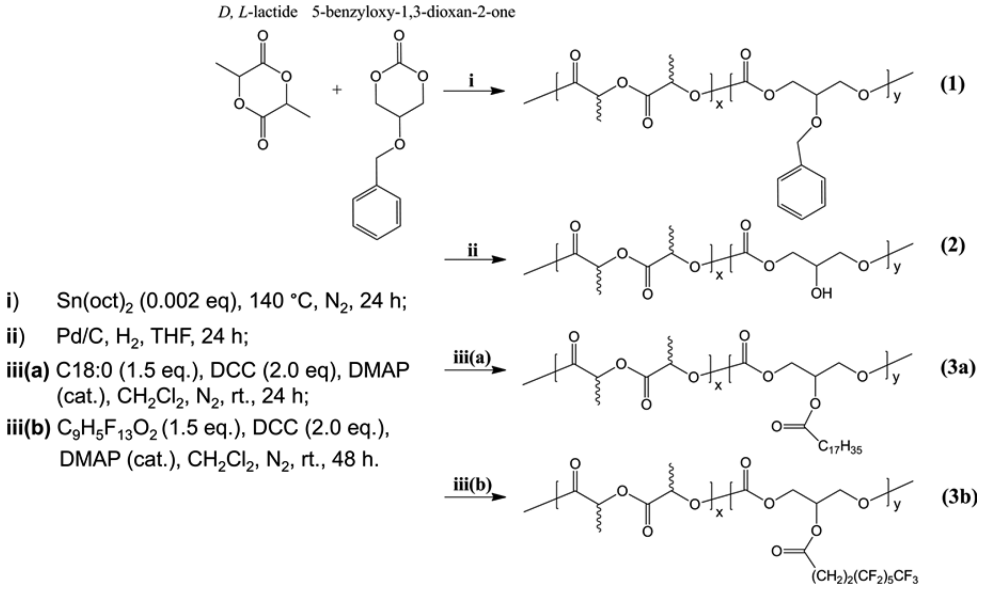

biodegradable polyesters such as PLGA (4 to 5 months for the 75:25 copolymer, for example).[37,38] In addition to a difference in degradation rate, PCL and PLGA differ in their degree of cystallinity: PCL is a semicrystalline polymer, whereas PLGA is amorphous; they also differ in mechanical properties.[38] Therefore, the goal of this study is to fabricate superhydrophobic electrospun meshes from PLGA doped with a family of new biodegradable hydrophobic poly(ester carbonate) copolymers to assess the relationships between copolymer composition, percent doping, fiber size, and wettability, and to provide a broad-based strategy for the design and fabrication of three-dimensional biodegradable polymer meshes as superhydrophobic biomaterials.

EXPERIMENTAL SECTION

Synthesis (Scheme 1). All reagents were used as received without further purification or modification, and the complete synthetic details and materials can be found in the Supporting Information. Briefly, the co-monomer, 5-benzyloxy-1,3-dioxan-2-one, was synthesized according to a literature procedure and recrystallized twice from dichloromethane/ether prior to use.[29] Polymerization was carried out on a 10 mmol overall scale at 140 °C under a nitrogen atmosphere in a tin-catalyzed ring-opening polymerization to afford poly(D,L-lactide-*co*-5-benzyloxy-1,3-dioxan-2-one) (polymer **1**). ^{1}H NMR integrations of the lactide and benzyl methylene protons were compared to determine copolymer composition. The benzyl protecting group of polymer **1** was subsequently deprotected using Pd/C hydrogenolysis to afford poly(D,L-lactide-*co*-5-hydroxy-1,3-dioxan-2-one) (polymer **2**). Lastly, pendant hydrophobic side chains of either stearic acid or 2*H*,2*H*,3*H*,3*H*-perfluorononanoic acid were attached to the free hydroxyl of polymer **2** in a DCC coupling reaction. The solution was then filtered, concentrated, and precipitated into methanol to afford poly(D,L-lactide-*co*-glycerol monostearate) and poly(D,L-lactide-*co*-glycerol-perfluorononanoate) (polymers **3a** PLA−PGC$_{18}$ and **3b** PLA−PGC$_{13F}$, respectively). The copolymer ratio was varied between 60:40 and 90:10 (PLA:PGC).

Instrumentation. ^{1}H and ^{13}C NMR spectra were recorded at 93.94 kG (^{1}H, 400 MHz; ^{13}C, 100 MHz) at ambient temperature. Proton chemical shifts are expressed in parts per million (ppm) relative to the residual proton solvent resonance: $CDCl_3$ δ = 7.24. For ^{13}C spectra, the centerline of the solvent signal was used as internal reference: $CDCl_3$ δ = 77.16. Thermal analysis of copolymers was performed using a Q100 differential scanning calorimeter (TA Instruments, DE, USA). Thermal traces were recorded for three steps: (1) heating to 225 °C at 10 °C/min, (2) cooling to −75 °C at 5 °C/min, and (3) heating to 225 °C at 10 °C/min. The second heating step (step 3) was used to identify phase and/or glass transition temperatures of the polymers. Mesh topography and fiber morphology were characterized using a Supra V55 (Carl Zeiss, Germany) field-emission scanning electron microscope operated at 2 kV. The static, advancing, and receding apparent water contact angle measurements were performed using a DSA100 (Kruss, NC, USA) to assess mesh wettability, and droplet (4 μL, n = 10) contact angles were calculated using the sessile drop (static) and T-2 (advancing and receding) fit methods. Mechanical analysis of the meshes was performed using a 5848 Microtester (Instron, MA, USA) in accordance with ASTM standard D882 for thin plastic sheeting, using a constant strain rate of 0.05/s.

Electrospinning. PLGA served as the major constituent of the polymer blends due to its high molecular weight and consequent high viscosity to afford chain entanglements and hence the ability to be efficiently electrospun. The synthesized copolymers, PLA−PGC$_{18}$ (90:10), PLA−PGC$_{18}$ (60:40), PLA−PGC$_{13F}$ (60:40), and PLA−PGC-OH, were used as PLGA dopants for the electrospinning. All polymers were dissolved in a mixture of THF/DMF (7:3) and thoroughly mixed before loading into a 15 mL glass syringe. The syringe was placed into a syringe pump and immediately electrospun from the tip of a 20G blunt needle at 3 mL/h, 7.5−15 kV. The resulting fiber jet was collected onto a grounded rotating and translating aluminum drum to collect a large mesh of uniform thickness (300 μm). Meshes were allowed to air dry at room temperature overnight before performing subsequent characterization.

***In Vivo* Foreign Body Response in Mice.** The animal experimental protocol was approved by the Institutional Animal Care and Use Committee of Dana Farber Cancer Institute and Boston University. The biocompatibility of the undoped PLGA, PLGA + 30% PLA−PGC$_{18}$ (60:40), and PLGA + 30% PLA−PGC$_{13F}$ (60:40) meshes was assessed in C57BL/6 female mice (Jackson Laboratory, Bar Harbor, ME). To test whether surface topography impacted biocompatibility (i.e., fibrous capsule thickness and foreign body reaction), smooth films of corresponding composition (undoped PLGA and PLGA + 30% PLA−PGC$_{18}$ (60:40)) were prepared from their mesh counterparts by heating until the fibers coalesced into a homogeneous, viscous transparent film that hardened upon cooling. The skin of the mice was shaved and aseptically prepared followed by a 0.5 cm incision that was made under isoflurane (1.0−1.5%) inhalation anesthesia. A subcutaneous pocket was made by blunt dissection. Films and meshes were cut to 0.6 × 0.6 cm^2 rectangles, sterilized by

dx.doi.org/10.1021/bm500410h | *Biomacromolecules* 2014, 15, 2548−2554

Table 1. Composition and Properties of Synthesized Copolymers

copolymer	conversion (%)	lactide[a]	glycerol[a]	M_n (g/mol)[b]	M_w/M_n	T_g (°C)[c]	T_m (°C)	T_c (°C)	ΔH_f (J/g)
PLA–PGC_{18} (90:10)	92	89	11	12 512	1.5	28			
PLA–PGC_{18} (80:20)	96	78	23	10 979	1.5	17	33	11	3.0
PLA–PGC_{18} (70:30)	90	66	34	17 305	1.5	[d]	40	17	23
PLA–PGC_{18} (60:40)	86	54	47	13 226	1.6	[d]	43	27	32

[a]Mole %. [b]As determined by size-exclusion chromatography (THF, 1.0 mL/min); M_n = number-average molecular weight; M_w/M_n = dispersity. [c]T_g = glass transition temperature; T_m = melting temperature; T_c = crystallization temperature; ΔH_f = heat of fusion. [d]No T_g was observed for these semicrystalline polymers over the temperature range from −75 to 225 °C.

ultraviolet irradiation, and then randomly implanted on the upper or lower back of C57BL/6 female mice such that each mouse received two different film/mesh types. After closure of the incision with 5-0 polypropylene sutures, mice were monitored until full recovery from anesthesia. After 4 weeks postimplantation, the meshes and surrounding tissue were carefully harvested after euthanasia, and cross-sections were prepared by paraffin embedding and H&E staining. Optical microscopy was performed on an Olympus BX41 microscope with an attached Olympus DP70 digital camera using an automated exposure setup.

RESULTS AND DISCUSSION

A family of new aliphatic poly(ester carbonates), poly(D,L-lactide-*co*-glycerol monostearate), was synthesized neat and in good conversion (~90%) from the racemic lactide monomer and 5-benzyloxy-1,3-dioxan-2-one at 140 °C using a tin-catalyzed ring-opening polymerization (Scheme 1). Monomer composition was varied to produce copolymers with 10, 20, 30, and 40 mol percent glycerol carbonate (GC), which was confirmed using ^{1}H NMR analysis by comparing peak integrations between the benzyl protecting group ($-CH_2$) of GC and the lactide backbone ($-CH_2$). Subsequent deprotection using Pd/C-catalyzed hydrogenolysis afforded a secondary alcohol that was coupled to stearic acid using a standard DCC procedure in order to enhance hydrophobicity (~90% yield).

Molecular weights of these C_{18}-derivatized polymers were relatively similar (10–17 kg/mol, M_w/M_n ~1.5), which facilitated comparison of thermal properties using differential scanning calorimetry (DSC). At low C_{18} content (i.e., PLA–PGC_{18} (90:10)), the copolymer is amorphous, having a glass transition (T_g) of 28 °C and no melting or crystallization event. Crystallinity increases as the C_{18} content increases from 20 to 40% (Table 1), as evidenced by the appearance of crystallization and melting peaks and increasing heats of fusion. Melting transitions (T_m) for these polymers also increased with increasing C_{18} content, which is likely due to the close, ordered packing of the hydrocarbon chains within the polymer and is partially supported by the observation that the free hydroxyl [PLA-OH (60:40)] copolymer is amorphous, T_g = −7 °C (see Supporting Information).

Electrospinning is a versatile polymer processing method by which nonwoven nano- and microfiber meshes with high surface area and surface roughness are prepared from polymer melts,[39] solutions,[40] blends,[41] immiscible mixtures,[42] emulsions,[43] and even from low-molecular-weight supramolecular assemblies.[44] We therefore hypothesized that electrospinning THF/DMF solutions (7:3) of PLGA 75:25 (MW = 129 kg/mol, M_w/M_n = 1.6) doped with varying amounts of PLA–PGC_{18} copolymers will alter the hydrophobicity of the material and, through optimization, will afford three-dimensional microfiber meshes with superhydrophobic characteristics. Specifically, we investigated how the C_{18} content of the PLA–PGC_{18} copolymer, dopant concentration, and fiber size of electrospun meshes affected wettability.

Electrospinning was accomplished by loading these polymer solutions into a syringe configured in a syringe pump (Q = 3.0 mL/h) and applying a high voltage to the tip of the syringe needle as the solution was collected onto a rotating drum. Fiber size was controlled by varying the total polymer concentration of the solutions: 30 wt % solutions resulted in small (2.5–3.5 μm) diameter fibers, whereas 40 wt % solutions resulted in large (6.5–7.5 μm) fibers (Figure 1). The polymer dopants

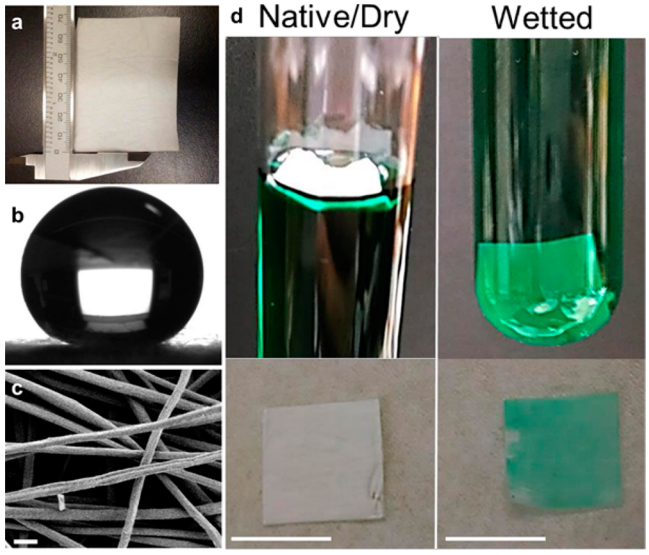

Figure 1. Superhydrophobic PLGA mesh doped with 30% PLA–PGC_{18} (60:40): (a) photograph of a mesh, (b) water droplet on a mesh surface showing a contact angle of 160°, and (c) low-magnification SEM of a mesh (scale bar = 10 μm). (d) Illustration of the bulk superhydrophobicity of the mesh, where a nonwetted mesh floats on water (colored green with dye to increase contrast), whereas an ethanol-wetted mesh placed in water sinks to the bottom. Dry and wetted meshes removed from the water are white and green, respectively (scale bar = 1 cm).

selected for electrospinning with PLGA were the PLA–PGC_{18} (90:10) and PLA–PGC_{18} (60:40) copolymers, and SEM images of all of the meshes can be found in Figures 1, S1, S2, and S3. We hypothesized that increasing copolymer composition (i.e., C_{18} content) would raise the apparent water contact angle to afford superhydrophobic meshes. The apparent advancing and receding water contact angles on large-fiber electrospun pure PLGA meshes were ~110 and 81°, and the contact angle increased as fiber size was reduced or as copolymer doping was increased such that advancing contact angles as high as ~162° (and receding as high as 145°) were obtained for small-fiber PLGA doped with 30% PLA–C_{18}

dx.doi.org/10.1021/bm500410h | Biomacromolecules 2014, 15, 2548–2554

(60:40) (Figures 1 and 2; see Figure S4 for the static contact angles). The difference between the values (i.e., hysteresis) for

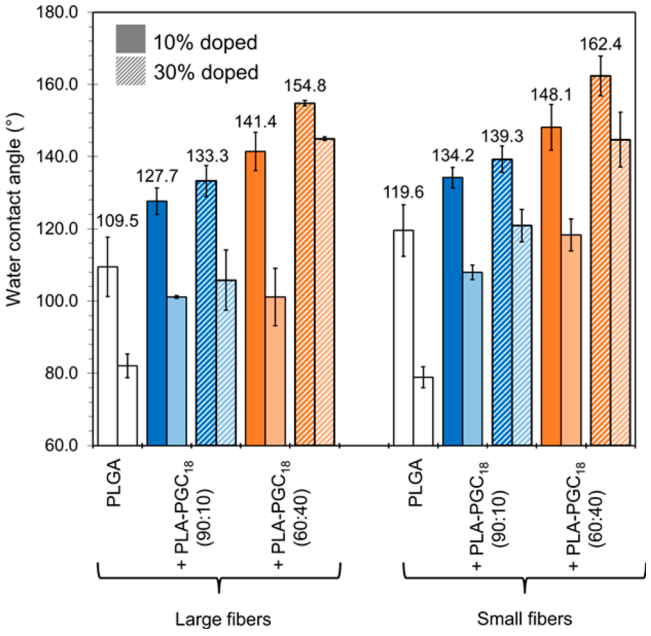

Figure 2. Influence of fiber size, copolymer dopant species, and percent doping on the apparent advancing (dark shade) and receding (light shade) water contact angles of PLGA-based microfiber meshes (PLGA, white; PLA-PGC_{18} (90:10), blue; PLA–PGC_{18} (60:40), orange). Error bars represent standard deviation (n = 10).

the advancing and receding contact angles decreased once the materials transitioned from hydrophobic to superhydrophobic. Reducing the fiber diameter enhanced mesh hydrophobicity (i.e., greater apparent advancing and static water contact angles) by decreasing the polymer surface fill fraction and increasing the air fraction exposed at the surface. Likewise, minimizing the mesh surface roughness via melting the meshes into films also dramatically reduced the water contact angles to 100° or lower for the respective compositions (see Supporting Information Figure S5). The degree of hydrophobicity was also dependent on dopant copolymer composition, with an increase in hydrophobicity as the lactide–C_{18} ratio increased (Figure 2). In contrast, electrospun meshes doped with 30% of the free hydroxyl copolymer PLA–PGC-OH (60:40) did not appreciably enhance mesh hydrophobicity (WCA ≈ 120 ± 4° for 2.5–3.5 μm fibers; Supporting Information Figure S3), confirming that the enhancement in hydrophobicity was due to the C_{18} moiety. The fibers within these meshes were relatively smooth and randomly oriented, as revealed by scanning electron microscopy. However, in the extreme case of small fibers doped with 30% PLA–PGC_{18} (60:40), a tertiary web-like structure developed on the fiber surface, adding to the overall surface roughness and resulting in a high apparent contact angle (Figure 3b).

Doped PLGA meshes were also assessed for cytotoxicity and biodegradability. Co-incubation of PLGA or 30% doped meshes with NIH/3T3 cells showed no loss of viability (viability > 95%, see Supporting Information Figure S6) after 24 h, as determined using the MTS colorimetric viability assay and compared to that of the untreated controls. The degradation half-life (in PBS at 37 °C) of the meshes occurred around 20–25 weeks (see Supporting Information Figure S7). Differences in degradation after 25 weeks were noted. For example, the 30% doped PLA–PGC_{18} (60:40) meshes were more resistant to degradation, losing only ∼35–40% of their mass, compared to ∼65–75% mass lost for pure PLGA meshes, after 25 weeks. The reduced hydrolytic degradation of PLA–PGC_{18} doped PLGA meshes may be due to the greater degree of crystallinity of the PLA–PGC_{18} copolymer (Table 1) and the greater mole fraction of PGC_{18} monomer units (i.e., greater number of carbonate linkages and hydrophobic C_{18} pendant groups) in these meshes. The pendent C_{18} is grafted to the polymer backbone by a hydrolzyable ester linkage, providing a mechanism for polymer degradation. This result is consistent with the literature reports that observed slower degradation rates of PLGA samples having higher degrees of crystallinity[45] and that polycarbonates, in general, degrade slower than polyesters.[46] However, because the overall molar percentage of PGC_{18} monomers was 3× lower in the 10% doped meshes and even lower for PLA–PGC_{18} (90:10) doped meshes, there were no discernible differences in the degradation trends for the other mesh compositions.

In addition to generating superhydrophobic meshes through the addition of PLA–PGC_{18} copolymer dopants to PLGA, we investigated whether grafting other hydrophobic moieties on the polymer backbone can impart superhydrophobicity, such as a perfluoroalkyl pendant chain. A poly(D,L-lactide-*co*-glycerol-2-2*H*,2*H*,3*H*,3*H*-perfluorononanoate) [PLA–PGC_{13F} (60:40)] copolymer was therefore synthesized in a similar manner as that of PLA–PGC_{18} and subsequently doped into a solution of PLGA and electrospun. At a 30% doping level, these perfluoroalkyl doped microfiber (2.5–3.5 μm; see Figures 3 and S3) meshes exhibited contact angles of ∼148°, which is lower than that observed with the C_{18} copolymer analogue (∼160°). We attribute the higher pure water contact angle for the PLA–PGC_{18} (60:40) doped PLGA mesh to the greater surface roughness present on these fibers compared to those fibers in the PLA–PGC_{13F} (60:40) doped PLGA mesh (Figure 3).

Considering the role of surface tension and surface energy on the wettability of superhydrophobic materials, we further explored wettability parameters by varying the surface tension of water by creating ethanol–water mixtures of known surface tension[47] and measuring the contact angle of these droplets on the most superhydrophobic 30% PLA–PGC_{18} (60:40) and PLA–PGC_{13F} (60:40) doped PLGA meshes. Despite having a higher apparent pure water contact angle, the PLA–PGC_{18} doped PLGA mesh was unable to support droplets with surface tensions below 36 mN/m, whereas the PLA–PGC_{13F} doped PLGA mesh maintained droplets with surface tensions as low as 23 mN/m (Figure 3). A possible explanation for why the PLA–PGC_{13F} doped PLGA mesh can support a lower surface tension liquid compared to that of the PLA–PGC_{18} doped PLGA mesh is that the smooth conformal coating present on the PGC_{13F} doped PLGA fibers prevents ethanol absorption by the polylactic acid better than that of the rough porous coating present in the PLA–PGC_{18} doped PLGA meshes.

Next, uniaxial tensile testing on the meshes was performed to determine the effect of PLA–PGC_{18} copolymer dopant and/or fiber size on the mechanical properties (elastic modulus, ultimate tensile strength, and strain at failure) of the PLGA meshes (Table 2). A trend was observed of decreasing stiffness and strength with increased doping and reduced fiber size. However, this was not the case for meshes doped with 30% PLA–PGC_{18} (90:10), as this formulation showed enhanced

dx.doi.org/10.1021/bm500410h | *Biomacromolecules* 2014, 15, 2548–2554

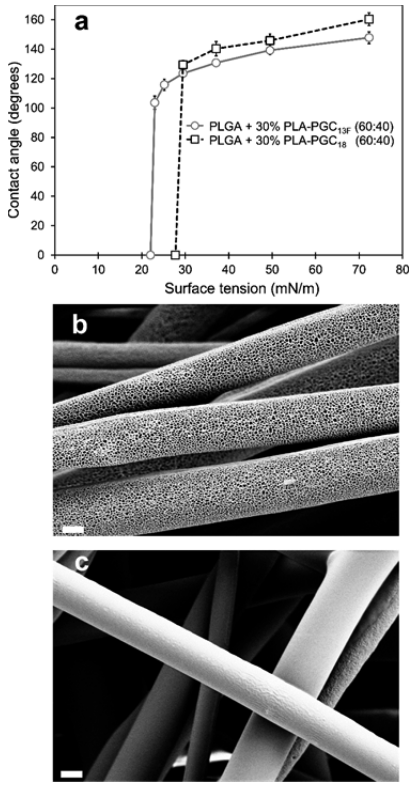

Figure 3. (a) Contact angle as a function of droplet surface tension for PLGA meshes doped with 30% PLA–PGC_{18} (60:40) and PLA–PGC_{13F} (60:40). Fiber size was 2.5–3.5 μm for both meshes (scale bar = 1 μm; error bars represent standard deviation for 10 droplet measurements). (b) High-magnification SEM of PLGA mesh doped with 30% PLA–PGC_{18} (60:40) showing high surface roughness compared to (c) fibers fabricated from PLGA doped with 30% PLA–PGC_{13F} (60:40), which have smooth fibers.

mechanical strength and stiffness compared to that of undoped PLGA meshes, and warrants further study. This composition also had a 20–25° increase in contact angle compared to that of PLGA and may be an appropriate material for providing enhanced hydrophobicity of PLGA without sacrificing mechanical strength, such as for surgical buttressing materials.

The *in vivo* biocompatibility and foreign body reaction to electrospun meshes were assessed 4 weeks after subcutaneous implantation in mice (Figures 4 and 5). A separate group of meshes was melted to eliminate surface roughness and therefore act as a nonsuperhydrophobic control with identical polymer composition. In general, meshes experienced a greater

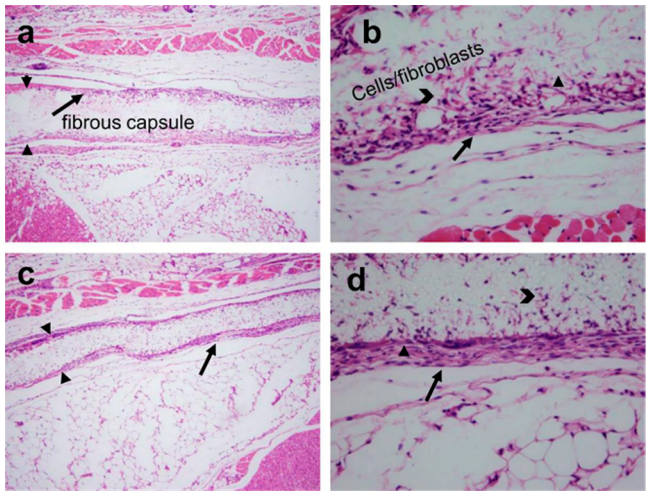

Figure 4. Histological (H&E) specimens of harvested subcutaneous mouse tissue surrounding implanted superhydrophobic meshes after 4 weeks. Superhydrophobic PLGA + 30% PLA–PGC_{18}(60:40) mesh at (a) 10× and (b) 40× magnifications. Superhydrophobic PLGA + 30% PLA–PGC_{13F} (60:40) mesh at (c) 10× and (d) 40× magnifications.

degree of tissue ingrowth (arrows) by macrophages and fibroblasts compared to films, as may be expected given the greater degree of porosity. Nonetheless, all meshes and films (labeled with arrowheads) were well-tolerated in mice and showed minimal signs of fibrous encapsulation (arrows). Fibrous encapsulation is characteristic of a foreign body response to an implanted device.[48] A small number of macrophages are indeed present at 4 weeks after implantation as part of a mild inflammatory reaction. This is to be expected as part of the normal host response to an implanted material that persists to this time point. The foreign body response to the superhydrophobic meshes (Figure 4) was similar to that of implanted PLGA meshes and smooth (i.e., nonsuperhydrophobic) PLGA films doped with 30% PLA–PGC_{18} (60:40) (Figure 5). Furthermore, these results are similar to electrospun PCL meshes implanted in rats performed by Cao et al.[49] Their study also examined the effect of fiber orientation (i.e., random or aligned) on fibrous capsule thickness and foreign body giant cell count, and they concluded that the fibrous architecture was capable of minimizing the foreign body response compared to that of smooth films and that thinner fibrous capsules were observed for the aligned fiber meshes compared to that of the meshes with randomly oriented fibers.

Table 2. Mechanical Properties of Doped Electrospun PLGA Meshes

copolymer dopant	doping %	fiber size[a]	E (MPa)[b]	UTS (MPa)[c]	ε (break)[d] (%)
PLA–PGC_{18} (90:10)	10	large	166.2 ± 20	6.3 ± 0.3	12
	10	small	139.4 ± 15	2.9 ± 0.3	
	30	large	90.9 ± 3.4	2.4 ± 0.6	
	30	small	90.4 ± 5.5	3.0 ± 0.1	
PLA–PGC_{18} (60:40)	10	large	40.3 ± 8.9	0.8 ± 0.1	1.9
	10	small	46.5 ± 11	1.7 ± 0.2	31
	30	large	10.1 ± 4.4	0.3 ± 0.1	8.7
	30	small	1.1 ± 0.4	0.1 ± 0.01	
PLGA (undoped)	0	large	84.9 ± 15	2.6 ± 0.4	
	0	small	63.6 ± 11	2.5 ± 0.4	

[a]Large fibers: 6.5–7.5 μm; small fibers: 2.5–3.5 μm. [b]Elastic modulus. [c]Ultimate tensile strength. [d]Strain at failure.

dx.doi.org/10.1021/bm500410h | *Biomacromolecules* 2014, 15, 2548–2554

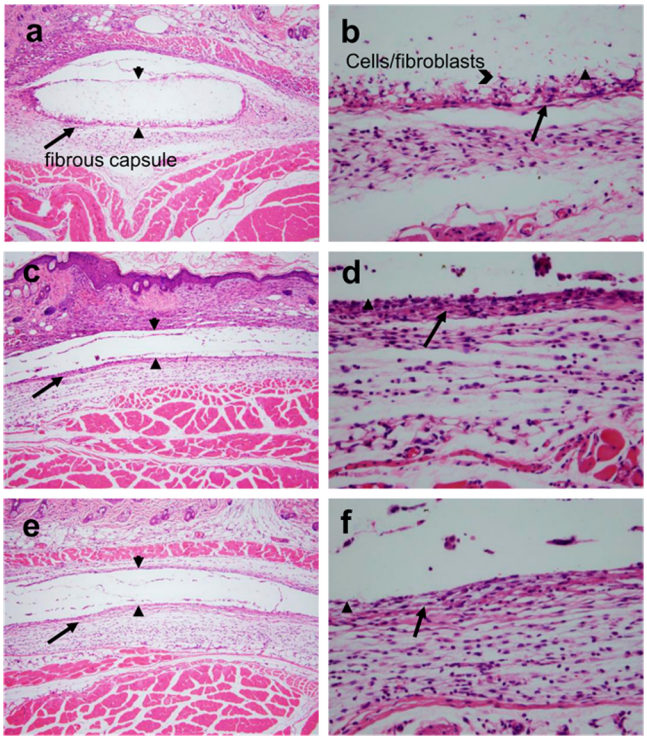

Figure 5. Histological (H&E) specimens of harvested subcutaneous mouse tissue surrounding implanted nonsuperhydrophobic meshes and films after 4 weeks. PLGA mesh at (a) 10× and (b) 40× magnifications. PLGA film at (c) 10× and (d) 40× manifications. Nonsuperhydrophobic PLGA + 30% PLA–PGC_{18} (60:40) film/melted mesh at (e) 10× and (f) 40× magnifications.

CONCLUSIONS

A series of polyester-carbonate copolymers based on D,L-lactide and glycerol is synthesized in good yield, with molecular weights of approximately 15 kg/mol. The ratio of glycerol to lactic acid is varied from 10 to 40%, and the pendant free hydroxyl on glycerol is subsequently functionalized with stearic acid to impart additional hydrophobicity to the copolymer (PLA–PGC_{18}). When these copolymers are added to a solution of PLGA at varying doping concentrations and the resulting mixture is electrospun, nonwoven microfiber meshes are fabricated with varying degrees of hydrophobicity. Mesh wettability is controlled through selection of fiber size, the amount of copolymer dopant added, and/or the lactide:C_{18} copolymer ratio. Hydrophobicity, as measured by apparent advancing contact angle, varied from of ∼110° for PLGA electrospun 7 μm fiber meshes to in excess of 160° for small-fiber meshes containing 30 wt % PLA–PGC_{18} (60:40). The degradation rate for the PLGA meshes doped with PLA–PGC_{18} (60:40) is slower than that for the PLGA meshes, and this is likely due to the greater degree of crystallinity, increased hydrophobicity (i.e., C_{18}), and the backbone carbonate linkages present within this polymeric mesh. In order to determine if this approach is generalizable, we replaced stearic acid with a perfluoroalkyl-based carboxylic acid, which is structurally and chemically different. The surface of the fibers ffrom the PLA–PGC_{13F} doped PLGA meshes are smoother than those from the PLA–PGC_{18} doped PLGA and thus these fluorinated meshes possess a lower apparent contact angle of ∼148°. The meshes fabricated in this work are noncytotoxic, as determined using the NIH/3T3 cell assay, and they do not elicit an adverse response when implanted *in vivo*. Given the potential toxicity of fluorinated polymers and their breakdown products,[50] additional *in vivo* studies over a longer duration are warranted for the perfluoroalkyl-grafted copolymer meshes prior to any biomedical use.

In summary, a robust and facile strategy to electrospin PLGA-based meshes is reported where the hydrophobicity of the mesh is tuned by choice of the polymer dopant, dopant concentration, and fiber size. Studies are ongoing to evaluate these meshes, composed of known biodegradable, biocompatible aliphatic polyesters and poly(ester carbonate)s, for drug delivery applications, where the surface and bulk properties are of particular importance for controlling drug release and cell/tissue integration, such as in a drug-eluting buttressing device that is implanted during surgical resection of early stage cancer.

ASSOCIATED CONTENT

Supporting Information

Synthesis of polymers; ^{1}H, ^{13}C, and ^{19}F NMR chemical shift assignments; cell viability assay; degradation study; contact angle study on smooth films and meshes; scanning electron micrographs for mesh formulations; and thermal and mechanical properties of PLGA meshes doped with 30% PLA-OH and 30% PLA-$(CF_2)_6CF_3$. This material is available free of charge via the Internet at http://pubs.acs.org.

AUTHOR INFORMATION

Corresponding Author

*E-mail: mgrin@bu.edu. Tel: (617)-358-3429. Fax: (617)-358-3186. Mailing address: Room 283, Metcalf Science and Engineering Center, 590 Commonwealth Avenue, Boston, Massachusetts 02215, United States.

Notes

The authors declare no competing financial interest.

ACKNOWLEDGMENTS

This work was supported in part by Boston University and the NIH (R01CA149561). H.L. acknowledges the Zhujiang Hospital, Southern Medical University, Guangzhou, China, for a fellowship opportunity with Brigham and Women's Hospital.

REFERENCES

(1) Tian, H. Y.; Tang, Z. H.; Zhuang, X. L.; Chen, X. S.; Jing, X. B. *Prog. Polym. Sci.* **2012**, *37*, 237–280.
(2) Emil, S. E.; Albert, P. R. Surgical Sutures. U.S. Patent 3,297,033, January 10, 1967.
(3) Greenberg, J. A.; Clark, R. M. *Rev. Obstet. Gynecol.* **2009**, *2*, 146–158.
(4) Weldon, C. B.; Tsui, J. H.; Shankarappa, S. A.; Nguyen, V. T.; Ma, M. L.; Anderson, D. G.; Kohane, D. S. *J. Controlled Release* **2012**, *161*, 903–909.
(5) Wright, J.; Hoffman, A. In *Long Acting Injections and Implants*; Wright, J. C., Burgess, D. J., Eds.; Springer: New York, 2012; pp 11–24.
(6) Wischke, C.; Schwendeman, S. P. *Int. J. Pharm.* **2008**, *364*, 298–327.
(7) Xie, J. W.; Tan, R. S.; Wang, C. H. *J. Biomed. Mater. Res., Part A* **2008**, *85A*, 897–908.
(8) Danhier, F.; Ansorena, E.; Silva, J. M.; Coco, R.; Le Breton, A.; Preat, V. *J. Controlled Release* **2012**, *161*, 505–522.
(9) Korin, N.; Kanapathipillai, M.; Matthews, B. D.; Crescente, M.; Brill, A.; Mammoto, T.; Ghosh, K.; Jurek, S.; Bencherif, S. A.; Bhatta,

D.; Coskun, A. U.; Feldman, C. L.; Wagner, D. D.; Ingber, D. E. *Science* **2012**, *337*, 738−742.
(10) Lee, J. S.; An, T. K.; Chae, G. S.; Jeong, J. K.; Cho, S. H.; Lee, H. B.; Khang, G. *Eur. J. Pharm. Biopharm.* **2005**, *59*, 169−175.
(11) Liu, H.; Wang, S. D.; Qi, N. *J. Appl. Polym. Sci.* **2012**, *125*, E468−E476.
(12) Ong, B. Y. S.; Ranganath, S. H.; Lee, L. Y.; Lu, F.; Lee, H. S.; Sahinidis, N. V.; Wang, C. H. *Biomaterials* **2009**, *30*, 3189−3196.
(13) Paun, I. A.; Moldovan, A.; Luculescu, C. R.; Staicu, A.; Dinescu, M. *Appl. Surf. Sci.* **2012**, *258*, 9302−9308.
(14) Alexis, F. *Polym. Int.* **2005**, *54*, 36−46.
(15) Li, S. M. *J. Biomed. Mater. Res.* **1999**, *48*, 342−353.
(16) Kumar, R.; Gao, W.; Gross, R. A. *Macromolecules* **2002**, *35*, 6835−6844.
(17) Seyednejad, H.; Ghassemi, A. H.; van Nostrum, C. F.; Vermonden, T.; Hennink, W. E. *J. Controlled Release* **2011**, *152*, 168−176.
(18) Wolinsky, J. B.; Ray, W. C.; Colson, Y. L.; Grinstaff, M. W. *Macromolecules* **2007**, *40*, 7065−7068.
(19) Barrera, D. A.; Zylstra, E.; Lansbury, P. T.; Langer, R. *J. Am. Chem. Soc.* **1993**, *115*, 11010−11011.
(20) Crick, C. R.; Parkin, I. P. *Chem.—Eur. J.* **2010**, *16*, 3568−3588.
(21) Li, X. M.; Reinhoudt, D.; Crego-Calama, M. *Chem. Soc. Rev.* **2007**, *36*, 1350−1368.
(22) Genzer, J.; Efimenko, K. *Biofouling* **2006**, *22*, 339−360.
(23) Ko, T.-J.; Kim, E.; Nagashima, S.; Oh, K. H.; Lee, K.-R.; Kim, S.; Moon, M.-W. *Soft Matter* **2013**, *9*, 8705−8711.
(24) Lourenco, B. N.; Marchioli, G.; Song, W. L.; Reis, R. L.; van Blitterswijk, C. A.; Karperien, M.; van Apeldoorn, A.; Mano, J. F. *Biointerphases* **2012**, *7*, 1−11.
(25) Privett, B. J.; Youn, J.; Hong, S. A.; Lee, J.; Han, J.; Shin, J. H.; Schoenfisch, M. H. *Langmuir* **2011**, *27*, 9597−9601.
(26) Manna, U.; Kratochvil, M. J.; Lynn, D. M. *Adv. Mater.* **2013**, *25*, 6405−6409.
(27) Manna, U.; Lynn, D. M. *ACS Appl. Mater. Interfaces* **2013**, *5*, 7731−7736.
(28) Yohe, S. T.; Colson, Y. L.; Grinstaff, M. W. *J. Am. Chem. Soc.* **2012**, *134*, 2016−2019.
(29) Yohe, S. T.; Herrera, V. L. M.; Colson, Y. L.; Grinstaff, M. W. *J. Controlled Release* **2012**, *162*, 92−101.
(30) Yohe, S. T.; Kopechek, J. A.; Porter, T. M.; Colson, Y. L.; Grinstaff, M. W. *Adv. Healthcare Mater.* **2013**, *2*, 1204−1208.
(31) Nayak, B. K.; Caffrey, P. O.; Speck, C. R.; Gupta, M. C. *Appl. Surf. Sci.* **2013**, *266*, 27−32.
(32) Mizukoshi, T.; Matsumoto, H.; Minagawa, M.; Tanioka, A. *J. Appl. Polym. Sci.* **2007**, *103*, 3811−3817.
(33) Yohe, S. T.; Grinstaff, M. W. *Chem. Commun.* **2013**, *49*, 804−806.
(34) Cui, Y.; Paxson, A. T.; Smyth, K. M.; Varanasi, K. K. *Colloids Surf., A* **2012**, *394*, 8−13.
(35) Sas, I.; Gorga, R. E.; Joines, J. A.; Thoney, K. A. *J. Polym. Sci., Part B: Polym. Phys.* **2012**, *50*, 824−845.
(36) Yohe, S. T.; Freedman, J. D.; Falde, E. J.; Colson, Y. L.; Grinstaff, M. W. *Adv. Funct. Mater.* **2013**, *23*, 3628−3637.
(37) Middleton, J. C.; Tipton, A. J. *Biomaterials* **2000**, *21*, 2335−2346.
(38) Nair, L. S.; Laurencin, C. T. *Prog. Polym. Sci.* **2007**, *32*, 762−798.
(39) Dalton, P. D.; Joergensen, N. T.; Groll, J.; Moeller, M. *Biomed. Mater.* **2008**, *3*, 034109−034119.
(40) Reneker, D. H.; Yarin, A. L. *Polymer* **2008**, *49*, 2387−2425.
(41) Wei, M.; Kang, B. W.; Sung, C. M.; Mead, J. *Macromol. Mater. Eng.* **2006**, *291*, 1307−1314.
(42) Zhong, G.; Wang, K.; Zhang, L.; Li, Z.-M.; Fong, H.; Zhu, L. *Polymer* **2011**, *52*, 5397−5402.
(43) Xu, X.; Yang, L.; Xu, X.; Wang, X.; Chen, X.; Liang, Q.; Zeng, J.; Jing, X. *J. Controlled Release* **2005**, *108*, 33−42.
(44) McKee, M. G.; Layman, J. M.; Cashion, M. P.; Long, T. E. *Science* **2006**, *311*, 353−355.
(45) Tsuji, H.; Miyauchi, S. *Polym. Degrad. Stab.* **2001**, *71*, 415−424.
(46) Tokiwa, Y.; Calabia, B.; Ugwu, C.; Aiba, S. *Int. J. Mol. Sci.* **2009**, *10*, 3722−3742.
(47) Vazquez, G.; Alvarez, E.; Navaza, J. M. *J. Chem. Eng. Data* **1995**, *40*, 611−614.
(48) Anderson, J. M.; Rodriguez, A.; Chang, D. T. *Semin. Immunol.* **2008**, *20*, 86−100.
(49) Cao, H.; McHugh, K.; Chew, S. Y.; Anderson, J. M. *J. Biomed. Mater. Res., Part A* **2010**, *93A*, 1151−1159.
(50) Lau, C.; Anitole, K.; Hodes, C.; Lai, D.; Pfahles-Hutchens, A.; Seed, J. *Toxicol. Sci.* **2007**, *99*, 366−394.